Earth's Future

RESEARCH ARTICLE
10.1029/2020EF001736

Projected Changes in Reference Evapotranspiration in California and Nevada: Implications for Drought and Wildland Fire Danger

Daniel J. McEvoy[1,2], David W. Pierce[3], Julie F. Kalansky[3], Daniel R. Cayan[3], and John T. Abatzoglou[4]

[1]Division of Atmospheric Sciences, Desert Research Institute, Reno, NV, USA, [2]Western Regional Climate Center, Reno, NV, USA, [3]Division of Climate, Atmospheric Sciences, and Physical Oceanography, Scripps Institution of Oceanography, University of California, San Diego, San Diego, CA, USA, [4]Management of Complex Systems Department, University of California, Merced, Merced, CA, USA

Key Points:
- All climate models show increasing reference evapotranspiration (ET_0) through the end of the century
- Increased air temperature has the greatest contribution to projected ET_0 increases
- Extreme ET_0-based wildfire potential and 3-year droughts based on precipitation minus ET_0 become much more frequent in the future

Supporting Information:
- Supporting Information S1

Correspondence to:
D. J. McEvoy,
mcevoyd@dri.edu

Citation:
McEvoy, D. J., Pierce, D. W., Kalansky, J. F., Cayan, D. R., & Abatzoglou, J. T. (2020). Projected changes in reference evapotranspiration in California and Nevada: Implications for drought and wildland fire danger. *Earth's Future*, *8*, e2020EF001736. https://doi.org/10.1029/2020EF001736

Received 31 JUL 2020
Accepted 21 OCT 2020
Accepted article online 29 OCT 2020

Abstract Recent high impact wildfires and droughts in California and Nevada have been linked to extremes in the Evaporative Demand Drought Index (EDDI) and Standardized Precipitation Evapotranspiration Index (SPEI), respectively. Both indices are dependent on reference evapotranspiration (ET_0). Future changes in ET_0 for California and Nevada are examined, calculated from global climate model simulations downscaled by Localized Constructed Analogs (LOCA). ET_0 increases of 13–18% at seasonal timescales are projected by late century (2070–2099), with greatest relative increases in winter and spring. Seasonal ET_0 increases are most strongly driven by warmer temperatures, with increasing specific humidity having a smaller, but noteworthy, counter tendency. Extreme (95th percentile) EDDI values on the 2-week timescale have coincided with recent large wildfires in the area. Two-week EDDI extremes are projected to increase by 6–10 times during summer and 4–6 times during autumn by the end of the century. On multiyear timescales, the occurrence of extreme droughts based on 3-year SPEI below the historical fifth percentile, similar to that experienced during the 2012–2016 drought across the region, is projected to increase 3–15 times by late century. Positive trends in extreme multiyear droughts will further increase seasonal fire potential through degraded forests and increased fuel loads and flammability. Understanding how these drought metrics change on various climate timescales at the local level can provide fundamental information to support the development of long-term adaptation strategies for wildland fire and water resource management.

Plain Language Summary Since the start of the 21st century, California and Nevada have observed extreme wildland fires and droughts that have caused devastating impacts to ecosystems and society. A common feature of these events has been very high atmospheric evaporative demand—the "thirst" of the atmosphere—which has largely been driven by increased air temperatures caused by anthropogenic climate change. This study examines projected changes in evaporative demand, which of the input variables are causing those changes and how the frequency of extreme wildfire potential and multiyear droughts will change. Evaporative demand is found to increase during all seasons, and increased temperatures drive most of that change. The likelihood of extreme wildfire potential based on 2-week periods of elevated evaporative demand during summer and autumn increases substantially. A climatic water balance based on precipitation and evaporative demand indicates extreme 3-year droughts that hold potential to deplete regional-scale water supply also become much more likely. Future adaptation planning efforts for wildfire management agencies, forest management, and water resource managers should account for a greater likelihood of more extreme events.

1. Introduction

Wildland fires and droughts in California and Nevada have had devastating impacts on natural resources, ecosystems, and society. In the last decade, extreme events with unprecedented impacts have occurred including the 2012–2016 drought (e.g., Griffin & Anchukaitis, 2014; Lund et al., 2018; Shukla et al., 2015; Swain, 2015; Williams et al., 2015) and a series of catastrophic wildfires in 2017 and 2018 (Brown et al., 2020; Nauslar et al., 2018, 2019). A common thread in these recent events is the increased likelihood of exacerbated drought impacts and heightened fire potential due to increased air temperatures and

evaporative demand (E_0)—including that associated with anthropogenic climate change (e.g., Griffin & Anchukaitis, 2014; Goss et al., 2020; Shukla et al., 2015; Williams et al., 2015, 2019).

Evaporative demand (E_0)—the upper limit of actual evapotranspiration (ET) that could occur given unlimited surface water supply (Hobbins et al., 2017)—has a strong connection to drought and wildfire potential in the western United States (e.g., Abatzoglou & Kolden, 2013; Abatzoglou & Williams, 2016; Littell et al., 2016; McEvoy et al., 2016) and globally (e.g., Dai, 2011; Vicente-Serrano et al., 2010). In California and Nevada, elevated E_0 contributed to the 2012–2016 drought's severity (Hobbins et al., 2016; McEvoy et al., 2016; Shukla et al., 2015; Williams et al., 2015) and to wildfire potential (Brown et al., 2020; McEvoy et al., 2019; Nauslar et al., 2019). Although E_0 is sometimes calculated from temperature alone, a physically based E_0 formulation is critical to obtaining realistic estimates that include not only temperature changes but also the wind speed, humidity, and incoming shortwave radiation components that drive land surface-atmosphere interactions and drying (Hidalgo et al., 2005; Hobbins et al., 2017). Reference ET (ET_0) calculated using the Penman-Monteith equation (Monteith, 1965) is a physically based formulation of E_0 that serves as the basis for the Evaporative Demand Drought Index (EDDI; Hobbins et al., 2016; McEvoy et al., 2016) and has been recommended as the E_0 component of the Standardized Precipitation Evapotranspiration Index (SPEI; Vicente-Serrano et al., 2010). While Hobbins (2016) has demonstrated that the historical (1981–2010) sensitivity of ET_0 to the drivers can vary regionally and seasonally, assessments that examine the sensitivity of ET_0 based on projected changes in the drivers are lacking.

A number of studies have looked at projected changes in ET_0 and drought indices that use ET_0 at global or Contiguous United States (CONUS) scale based on coarse resolution Global climate model (GCM) output (e.g., Cook et al., 2014; Dewes et al., 2017; Ficklin et al., 2016; Scheff & Frierson, 2014). More localized studies in portions of California and Nevada for specific basins or counties using downscaled GCM data have also been conducted (Huntington et al., 2015; Oakely et al., 2019). Using downscaled GCM data to develop ET_0 projections provides localized information about future fire potential and droughts that can highlight regional differences that are less apparent using coarser scale GCM data.

Extreme EDDI values (greater than 95th percentile) have been found to occur simultaneously with start dates of recent large and destructive wildfires in California (Brown et al., 2020; McEvoy et al., 2019; Nauslar et al., 2019) and has been put into use by fire management agencies (McEvoy et al., 2019). In addition to the aforementioned case studies, McEvoy et al. (2019) compared EDDI to seasonally averaged fire danger indices (ERC, 100-, and 1,000-hour fuel moisture) across California and Nevada for 1979–2015, and results show EDDI strongly reflects the buildup of antecedent drought conditions also found in dead fuel moisture. The multi-scalar nature of EDDI (Hobbins et al., 2016) and ability to decompose into individual weather drivers is appealing to fire managers who found added value when used in combination with traditional fire danger metrics (McEvoy et al., 2019). Abatzoglou and Kolden (2013) found ET_0 to have good interannual relationships to fire season total burned area in California. Several studies have examined climate change impacts on fire weather and fire danger indices in the region (Abatzoglou et al., 2019; Brown et al., 2004; Goss et al., 2020), but thus far, no studies have evaluated projected changes in extreme EDDI days for fire danger applications.

Multiyear droughts, particularly those lasting three or more years, have the greatest impact on California and Nevada water resources as even the larger reservoirs can become depleted causing water shortages for agriculture and public use (Lund et al., 2018) with the most devastating impacts to rural communities that rely on groundwater (Swain, 2015). Multi-scalar drought indices that incorporate both precipitation and ET_0 are better correlated to reservoir levels during droughts than indices only using precipitation, and levels in large reservoirs are best correlated at timescales of 3–4 years (McEvoy et al., 2012). While changes in annual SPEI have been examined globally (Cook et al., 2014), the occurrence of multiyear extreme droughts has not been examined using SPEI. Previous studies on changes in multiyear droughts have found increases in duration of soil moisture droughts in the Southwest United States (Cayan et al., 2010) and increased frequency of snow droughts in the western United States (Marshall et al., 2019).

This paper aims to build our understanding of how future changes in ET_0 can impact wildland fire potential and multiyear droughts in California and Nevada based on an ensemble of downscaled GCMs. Specifically, we seek to quantify changes in extreme ET_0 at short timescales for fire potential (2-week EDDI) and long timescales for sustained droughts (3-year SPEI). We first examine seasonal changes in precipitation, ET_0,

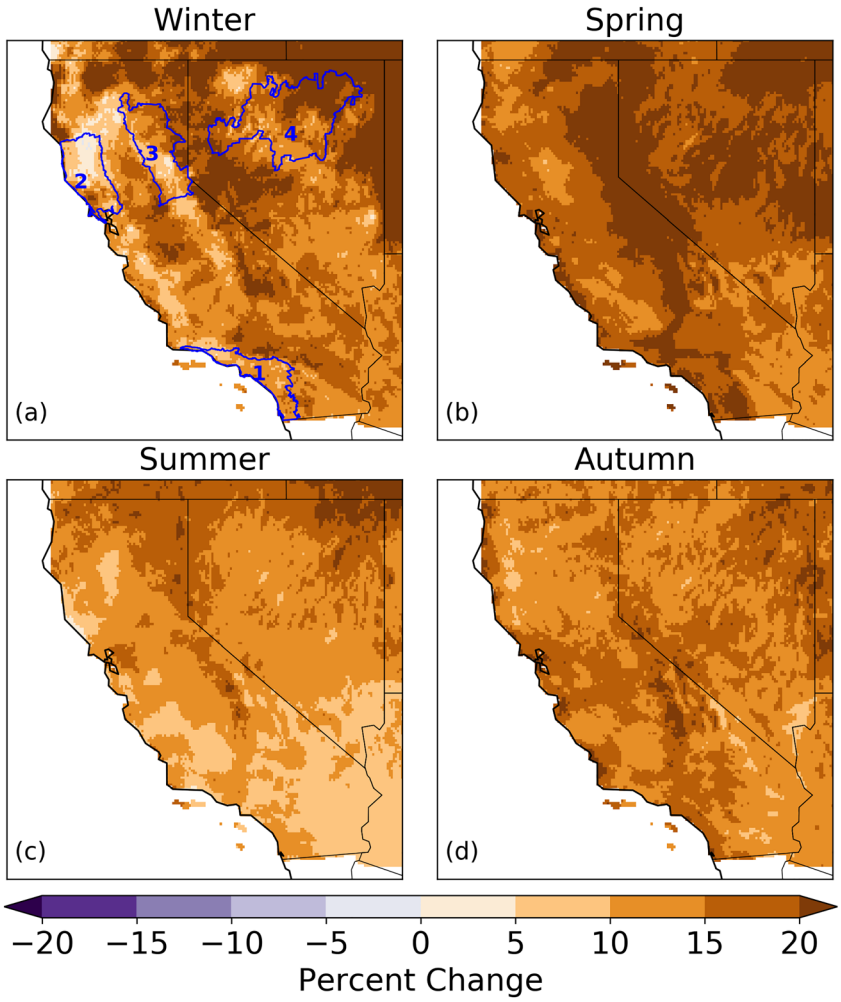

Figure 1. Seasonal LOCA RCP 8.5 ensemble median percent change in ET_0 for the late century period (2070–2099) relative to the base period (1950–2019) in (a) winter, (b) spring, (c) summer, and (d) autumn. Blue boundaries in (a) show Predictive Service Areas used in the study including (1) South Coast, (2) Mid Coast to Mendocino, (3) Northern Sierra in California, and (4) Humboldt Basin in Nevada.

and the drivers of ET_0. Second, we look at changes in extreme EDDI days as a metric of changes in wildfire potential. Finally, changes in multiyear droughts are assessed based on the 3-year SPEI and Standardized Precipitation Index (SPI).

2. Data and Methods

2.1. Daily Reference Evapotranspiration

To characterize historical changes in frequency of extreme EDDI days, daily ET_0 data were obtained from gridMET (Abatzoglou, 2013), which combines the North American Land Data Assimilation System version 2 and the Parameter Regression on Independent Slopes Model (PRISM) to produce continually updated daily data at 4 km spatial resolution over CONUS beginning in 1979. ET_0 is computed using gridMET temperature, wind speed, specific humidity, and incoming shortwave radiation following the ASCE Penman-Monteith procedure (Walter et al., 2000).

Four Predictive Service Areas (PSAs), a management unit used by the National Interagency Fire Center and Predictive Services for monitoring and forecasting fire danger as well as allocating resources for fire suppression, were used as spatial averaging domains to investigate both historical and future changes in ET_0 and precipitation. South Coast, Mid Coast to Mendocino (hereafter Mid Coast), and Northern Sierra PSAs were used in California and Humboldt Basin PSA for Nevada (Figure 1a). All four PSAs have experienced large

and destructive wildfires both historically and recently (McEvoy et al., 2019). These regions also provide surface water to large populations and/or major regional agricultural areas, making them ideal for studying long-term hydrologic drought. Daily gridMET ET_0 spatially averaged to each PSA for the period 1979–2019 was extracted using Climate Engine (Huntington et al., 2017).

2.2. Monthly Reference Evapotranspiration and Precipitation

Historical multiyear droughts are characterized using monthly ET_0 and *Prcp* from Williams et al. (2020) covering the period 1901–2018. This data set merges a number of observation-based and reanalysis products to produce a continuous timeseries over North America at 1/4° spatial resolution. For further details, see Williams et al. (2020) supplemental material. Monthly data were spatially averaged over each PSA.

2.3. LOCA Projections

GCM simulations from the Climate Model Intercomparison Project version 5 (CMIP5; Taylor et al., 2012) statistically downscaled using Localized Constructed Analogs (LOCA; Pierce et al., 2014; Pierce et al., 2015) were obtained for California and Nevada from the LOCA database (http://loca.ucsd.edu). Daily data at 6 km spatial resolution from historical (1950–2005) and future (2006–2099) LOCA runs for Representative Concentration Pathway (RCP) 4.5 (supplemental material) and 8.5 were used. Climate variables of maximum temperature (T_{max}), minimum temperature (T_{min}), specific humidity (q; Pierce & Cayan, 2016), wind speed (u), incoming shortwave radiation (R_d), and precipitation (*Prcp*) were examined. The full suite of LOCA GCMs includes 32 models of which 10 were selected in previous studies as best suited to studies in California and Nevada on the basis of performance over the historical era and independence in model lineage (Cayan & Tyree, 2015; Pierce et al., 2018). The performance measures that were evaluated included accuracy in the global representation of air temperature, pressure, wind, and solar radiation patterns; western U.S. regional evaluations of temperature, precipitation, sea level pressure, and (due to their teleconnected importance to regional climate) El Niño/Southern Oscillation variability; and California state evaluation of dry and wet regimes, heat waves, and cold snaps (Cayan & Tyree, 2015). Seven of the 10 GCMs retained daily q, u, and R_d necessary to calculate ET_0 and were used in this study: ACCESS1-0, CanESM2, CNRM-CM5, GFDL-CM3, HadGEM2-CC, HadGEM2-ES, and MIROC5. Gridded daily ET_0 covering California and Nevada was calculated using the ASCE Penman-Monteith method (Walter et al., 2000) and archived for both RCPs and historical and future periods. All future changes were calculated relative to a base period of 1950–2019 and classified by early (2020–2039), mid (2040–2069), and late (2070–2099) 21st century. A comparison of LOCA seasonal ET_0 totals with gridMET shows that LOCA does well in capturing the seasonal cycles and variability (supporting information Figures S1 and S2).

Seasonal changes relative to the base period for LOCA *Prcp*, mean temperature (T_{mean}), q, u, R_d, and ET_0 were computed for early, mid, and late century. Changes are expressed as the percent difference from the base period for ET_0 and *Prcp* and absolute difference for other variables, for each future year and then averaged over each of the three future periods. Seasonal timeseries (three-month average for each year) for each of the four PSAs described in section 2 were spatially averaged from the LOCA grids to examine the seven-model ensemble distribution for each variable.

A sensitivity experiment was performed on the seasonal ET_0 timeseries to examine which of the four atmospheric drivers is responsible for the greatest influence on future ET_0 changes. For each PSA, daily T_{mean}, q, u, and R_d climatology were computed using the base period. Next, ET_0 was computed four times, each time holding three of the four atmospheric drivers to the daily climatological values and letting the other driver vary (e.g., Cook et al., 2014; Scheff & Frierson, 2014; Williams et al., 2015; Zhao & Dai, 2015). This was done through the full LOCA time period (1950–2099), and seasonal ET_0 values were summed from daily values. Contributions to the total ET_0 anomaly relative to 1950–2019 were estimated for each year and then averaged over future periods (method detailed in Figure S3 and associated text).

2.4. Drought Indices

We examine both 2-week and 3-year drought indices in this work for wildland fire potential and long-term drought, respectively. The EDDI was computed following Hobbins et al. (2016) using a 2-week timescale. This short timescale can be used to examine rapid onset drought, or flash drought, and has been found to be effective for fire danger monitoring (McEvoy et al., 2019). Both meteorological phenomena

(e.g., frontal passage and downslope wind events) and persistent weather patterns lasting days-to-weeks (i.e., blocking high pressure) impact fuel moisture and flammability and are reflected in the 2-week EDDI. Further, we find over 25% of seasonal burned area in summer and autumn occurs coincident with extreme 2-week EDDI days across much of the region (Figure S4). For each year, daily counts of 2-week EDDI exceeding the historical 95th percentile during summer (June–August) and autumn (September–November) were found. Percentiles are relative to each day, not all days of the year. For gridMET, the entire 1979–2019 distribution was used to calculate EDDI. For LOCA data EDDI was computed using a fixed base period of 1950–2019 to constrain the distribution to the observed past. Data for 2020–2099 were ranked relative to the base period and capped on the upper or lower end of the distribution. The number of days for each year and season when EDDI exceeds the base period 95th percentile was calculated and then averaged for each future period. Any given day above the 95th percentile is likely not independent from neighboring days above this threshold given the serial correlation in the daily timeseries.

Multiyear droughts were examined using the SPI (McKee et al., 1993) and SPEI (Vicente-Serrano et al., 2010). SPI is a multi-scalar drought index that considers only *Prcp*. SPEI incorporates the demand side of drought by using the climatic water balance ($Prcp - ET_0$) as input. Precipitation is the driving factor in multiyear hydrologic droughts with elevated ET_0 acting to exacerbate drought severity. We therefore use SPEI instead of EDDI to examine the impact of ET_0 on multiyear droughts. SPI and SPEI were standardized using a non-parametric approach (Farahmand & AghaKouchak, 2015), which helps overcome the limitations of using different distributions to fit different variables. This standardization method was adopted by Hobbins et al. (2016) for EDDI and used for EDDI, SPI, and SPEI calculations in this study.

We computed 3-year water year (36-month ending September 30) SPEI (SPEI-36) and SPI (SPI-36) timeseries for each PSA using spatially averaged *Prcp* and ET_0. McEvoy et al. (2012) found SPEI timescales of 30–60 months strongly correlated to interannual variability in large reservoirs in California and Nevada with extreme low SPEI values tracking droughts and low reservoir levels. We therefore use a 36-month timescale to represent water supply droughts in the region. The U.S. Drought Monitor (Svoboda et al., 2002) classifies extreme drought as third to fifth percentile and exceptional drought as <third percentile. We use SPEI <fifth percentile to determine historical and future changes in extreme droughts. For historical SPI and SPEI using data from Williams et al. (2020), 1901–2018 was used for the distributions at each PSA. For LOCA SPI and SPEI we used 1950–2019 as the base period, and data for 2020–2099 were ranked relative to the base period and capped on the upper or lower end of the distribution (same as EDDI). A long duration aggregation window (36 months) is inherently serial correlated, and years below the fifth percentile are often overlapping and not independent from one another. In addition to counting the number of values, the overlaps were also counted to distinguish events (any overlaps) from single year values.

3. Results

3.1. LOCA Seasonal Changes

The seven-model ensemble shows consistent increases in ET_0 by the end of century (Figure 1 for RCP 8.5; Figure S5 RCP 4.5; Table 1). Winter and spring show increases of >20% over large swaths of the domain (Figures 1a and 1b, respectively), which is partially a function of the climatologically lower historical values in these seasons. Summer ET_0 increases 10–15% over much of the domain with greater increases in the northern areas and a large area of lesser (5–10%) increases over southern areas (Figure 1c). Autumn changes of 10–20% (Figure 1d) are more uniformly distributed over the region.

Precipitation changes (Figure 2 for RCP 8.5; Figure S6 RCP 4.5; Table 1) are less consistent than ET_0 both spatially and by season, similar to previous studies (e.g., Pierce et al., 2018). Winter (Figure 2a) shows the most spatial coherence with increases over nearly the entire domain, with a large extent of >30% and 45–60% + increases over Nevada. Spring (Figure 2b) and autumn (Figure 2d) show similar spatial patterns where decreasing *Prcp* is found in California and southern Nevada and increases in central and northern Nevada. Summer changes are noisy over nearly all of California and northwest Nevada due to the Mediterranean climate and low (near zero for some locations) absolute values of *Prcp* during this season. There is some evidence that future summer changes in precipitation in this region may be associated with monsoon processes that are better resolved by finer spatial resolution dynamical downscaling, as opposed to statistically downscaled coarse-resolution GCMs (Pierce et al., 2013).

Table 1
LOCA Ensemble Median Seasonal ET_0 and Prcp Historical Climatology (1950–2019) and Late Century (2070–2099) Changes Spatially Averaged Over the Entire Domain

ET_0 and *Prcp* historical climatology and late century changes						
Season	ET_0 climatology (mm)	Δ ET_0 (mm)	Δ ET_0 (%)	*Prcp* climatology (mm)	Δ *Prcp* (mm)	Δ *Prcp* (%)
Winter	139	23	17	198	26	13
Spring	414	75	18	115	−13	−11
Summer	708	94	13	33	−6	−18
Autumn	343	50	15	92	−8	−9

Focusing on autumn since it is a key fire season and the start of the transition to the wet season, late century changes in *Prcp*, ET_0, and the drivers of ET_0 are shown in Figure 3 for the four PSAs. In addition to ensemble median, the spread is also shown to highlight uncertainty in projections, which arises from both natural climate variability and model uncertainty. All four PSAs show increased ET_0 with ensemble medians ranging from 13% to 16% across the PSAs and increases in all ensemble members, despite a modest spread in magnitude (Figure 3a). Changes in *Prcp* (Figure 3b) are more variable than ET_0 changes. However, for all regions

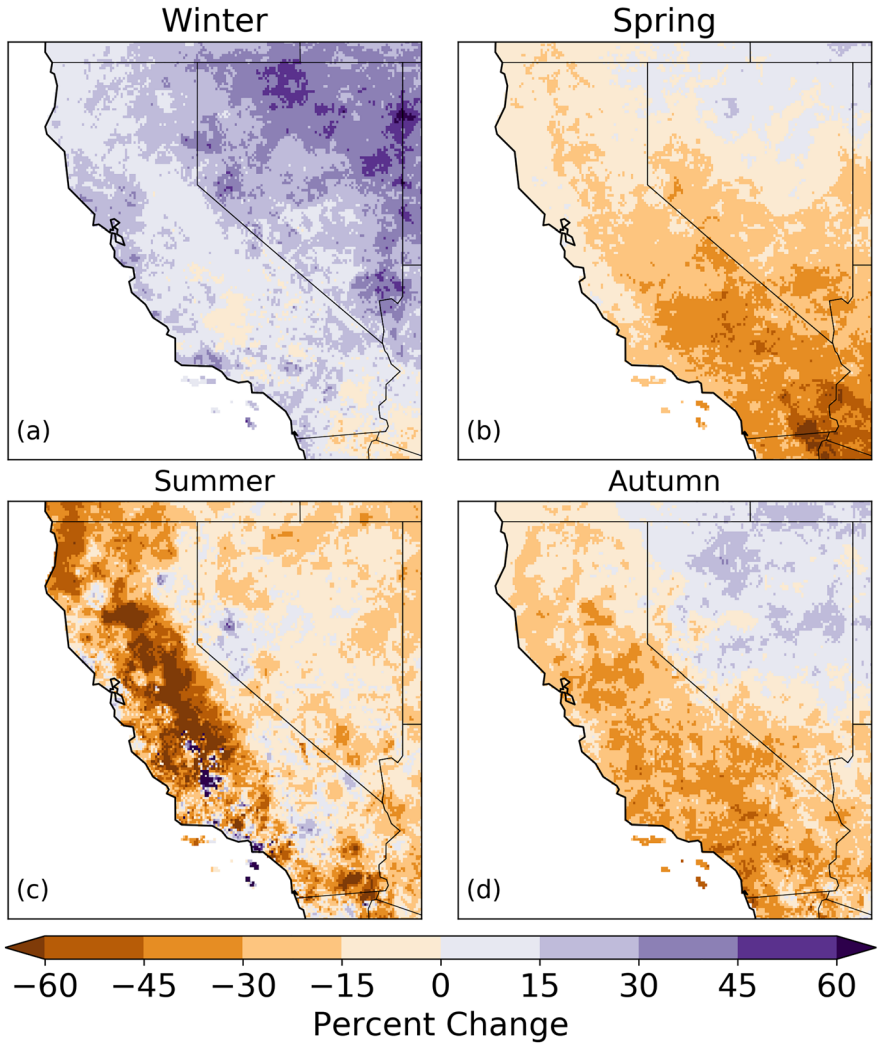

Figure 2. Seasonal LOCA RCP 8.5 ensemble median percent change in *Prcp* for the late century period (2070–2099) relative to the base period (1950–2019) in (a) winter, (b) spring, (c) summer, and (d) autumn.

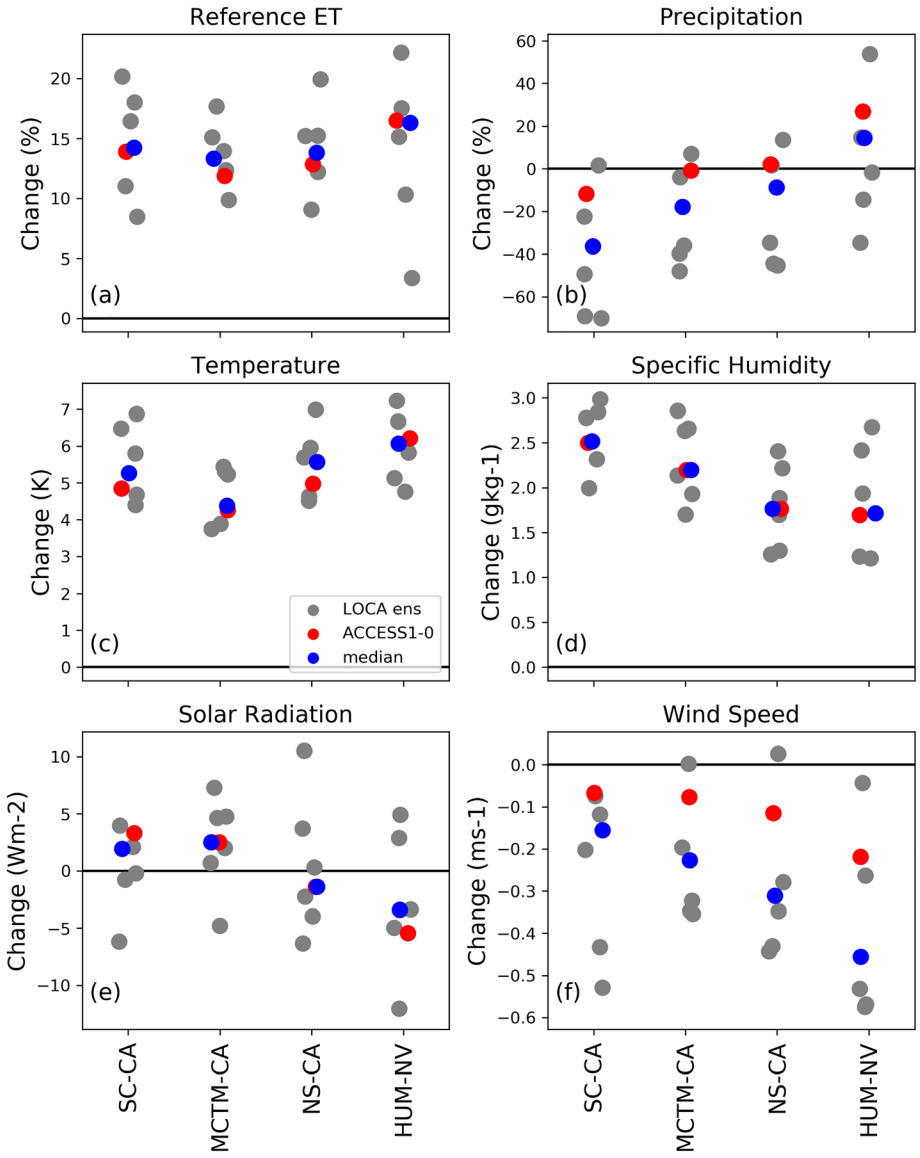

Figure 3. Autumn late century LOCA RCP 8.5 changes in (a) ET_0, (b) *Prcp*, (c) T_{mean}, (d) q, (e) R_d, and (f) u at four PSAs. In each panel the first column of dots is South Coast (SC-CA), second column is Mid Coast (MCTM-CA), third column is Northern Sierra (NS-CA), and fourth column is Humboldt Basin (HUM-NV). Gray dots show LOCA ensemble members, blue dots show ensemble median, and red dots show the ACCESS1-0 model results. ACCESS1-0 results are shown in Figure 4 as the ET_0 change for this model is near the median for select PSAs.

except for Humboldt Basin most ensemble members show drying. For Humboldt Basin, note that natural internal climate variability in regions where the mean change is projected to be near zero mandates that some models will show increasing *Prcp* while others show decreasing. Ensemble medians at all four PSAs show decreasing u (Figure 3f) and increasing q (Figure 3d) and T_{mean} (Figure 3c). Increasing ensemble median R_d was found at South Coast and Mid Coast, with decreases found at Northern Sierra and Humboldt Basin (Figure 3e), although the results are distributed around zero in the individual ensemble members. Other seasons show similar results for ET_0 and the drivers (not shown).

These tendencies are elucidated in the sensitivity experiments for autumn ET_0 using ACCESS1-0 (Figure 4), which has ET_0 changes near the middle of the ensemble distribution. In all regions T_{mean} contributes the most to ET_0 changes. The tendency from warming T_{mean} exceeds the actual ET_0 anomaly since there is an opposite tendency from increasing q. Projected q increases arise from increasing T_{mean}, but this sensitivity

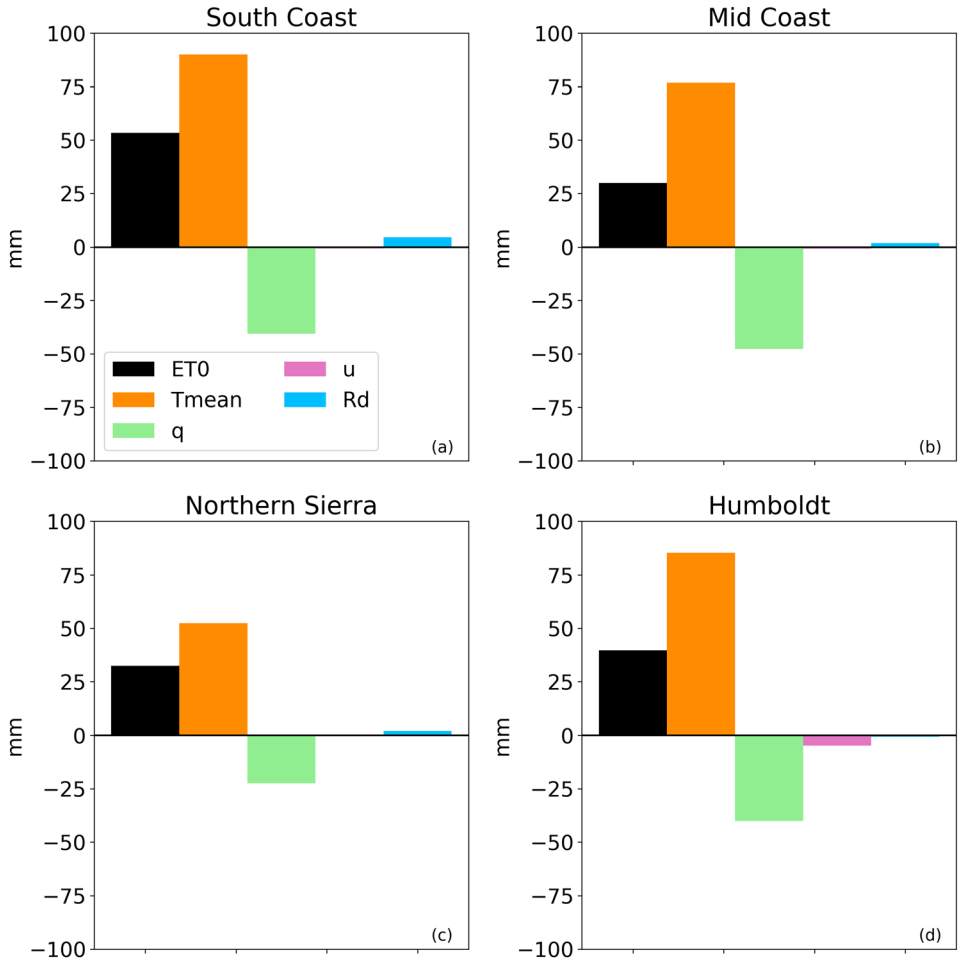

Figure 4. Autumn ET_0 anomaly and contributions from the four atmospheric drivers averaged over late century (2070–2099) from LOCA RCP 8.5 ACCESS1-0 at (a) South Coast, (b) Mid Coast, (c) Northern Sierra, and (d) Humboldt Basin. Anomalies were computed using the 1950–2019 base period.

analysis cannot account for the physical feedback between the two drivers. Contributions from u and R_d changes are much smaller than T_{mean} and q. Results from the other LOCA ensemble members were similar to ACCESS1-0, always finding T_{mean} to have the greatest contributions, with a smaller opposing tendency from q (Figure S7) and minimal impact from u and R_d. All other seasons have the greatest contributions from T_{mean} to the total ET_0 anomaly with notably smaller relative q contributions in summer compared to autumn (not shown).

3.2. Observed and Projected Changes in Extreme Fire Danger Based on the EDDI

The number of summer and autumn days with 2-week EDDI above the historical (1979–2019) 95th percentile value ($EDDI_{95}$) for each PSA are shown in Figure 5. Based on the 95th percentile statistic we should expect on average 4 days per year, per season above that threshold. Least-squares regressions indicate statistically significant ($p < 0.1$) increasing trends for Northern Sierra in summer and for South Coast, Mid Coast, and Northern Sierra in autumn. Notable for summer is the maximum counts (22 days) at Mid Coast occurred in 2018 when one of California's largest recorded wildfire complexes occurred—the Mendocino Complex (Figure 5c). For Northern Sierra summer far more consecutive years with $EDDI_{95}$ counts above zero are found starting in 2000 (Figure 5e). During autumn, the highest day count (31 days) at Mid Coast occurred in 2019 (Figure 5d). Similarly, Northern Sierra also experienced its greatest autumn day count (25 days) in 2019, and 14 days were observed in 2018 when the Camp Fire occurred, the most destructive wildfire in California's history. Fewer $EDDI_{95}$ days have occurred at Humboldt Basin in recent years with zero summer counts from 2017 to 2019 (Figure 5g) and zero autumn counts from 2015 to 2019 (Figure 5h).

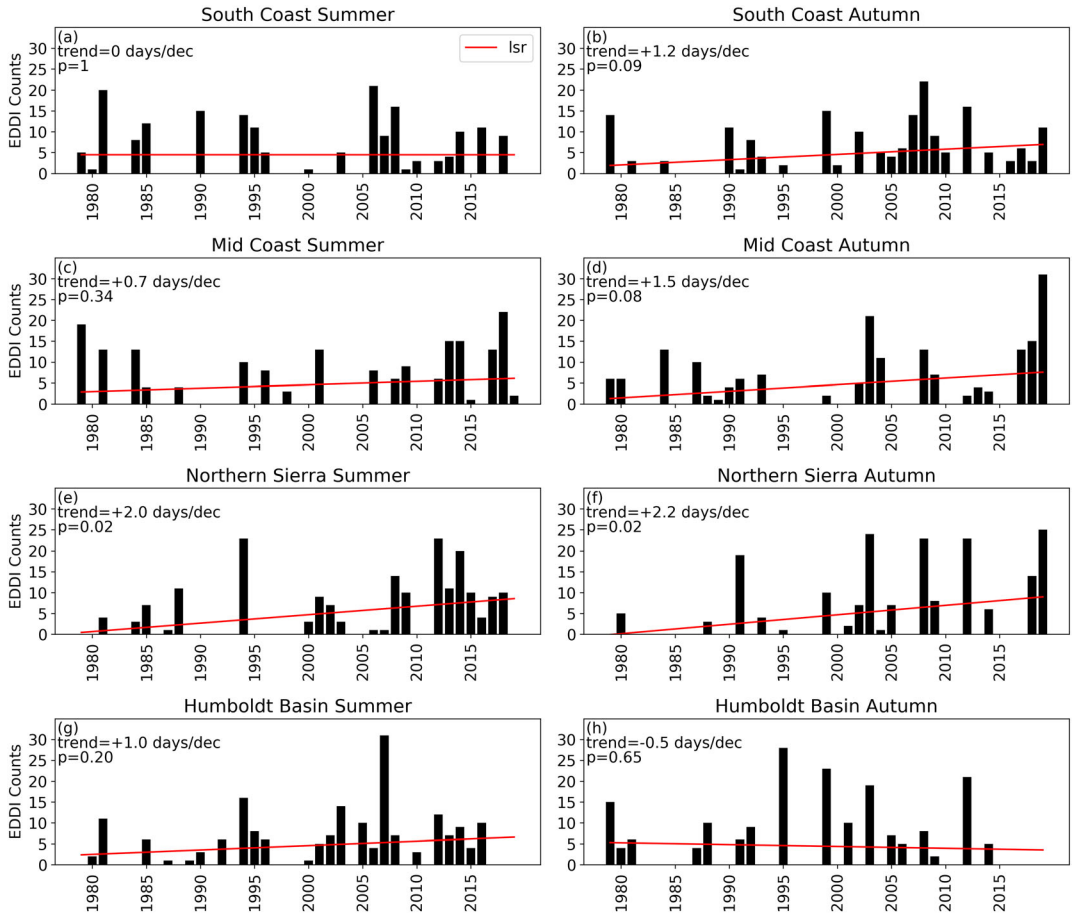

Figure 5. Historical (1979–2019) gridMET total counts of daily 2-week EDDI exceeding the 95th percentile value for (left column) summer and (right column) autumn at (a, b) South Coast, (c, d) Mid Coast, (e, f) Northern Sierra, and (g, h) Humboldt Basin. Red line in each panel shows the least square regression. Trends are reported in days per decade over the 41-year period.

LOCA projected change in the average number of summer and autumn $EDDI_{95}$ days per year in each future period is shown in Figure 6 for RCP 8.5 (Figure S8 RCP 4.5). Using the 1950–2019 LOCA baseline one would expect on average 5 days per year, per season above the 95th percentile. Note this is slightly different than the expected value of 4 days per year for gridMET in Figure 5 since the base periods are different. Increases in $EDDI_{95}$ days in summer and autumn are projected during the 21st century. Model medians project 30–48 summer $EDDI_{95}$ days per year and 23–26 autumn $EDDI_{95}$ days per year by late century, representing on average an eightfold and fivefold increase over baseline conditions, respectively. By late century the seasonal difference in day counts is particularly large at the South Coast and Northern Sierra regions. At the South Coast, the late century summer median day count is 47 compared to 26 days in autumn (Figure 6a), and at the Northern Sierra summer median day count is 52 compared to 23 days in autumn (Figure 6c). These results indicate a high likelihood of substantially more extreme 2-week EDDI days in summer and autumn relative to the base period which will contribute to more high fire danger days.

3.3. Observed and Projected Changes in Multiyear Droughts

Historical timeseries of SPI-36 and SPEI-36 for 1904–2018 at each PSA are shown in Figure 7. Similar prolonged drought periods are identified by SPEI and SPI but with differences in severity. In the 1950s SPI-36 shows more extreme values than SPEI-36, while in the mid-1990s onward the situation is reversed, with SPEI-36 showing more extreme values. In each region SPI-36 shows the lowest values not occurring during the 2012–2016 drought period, while SPEI-36 shows the lowest values during the 2012–2016 drought period

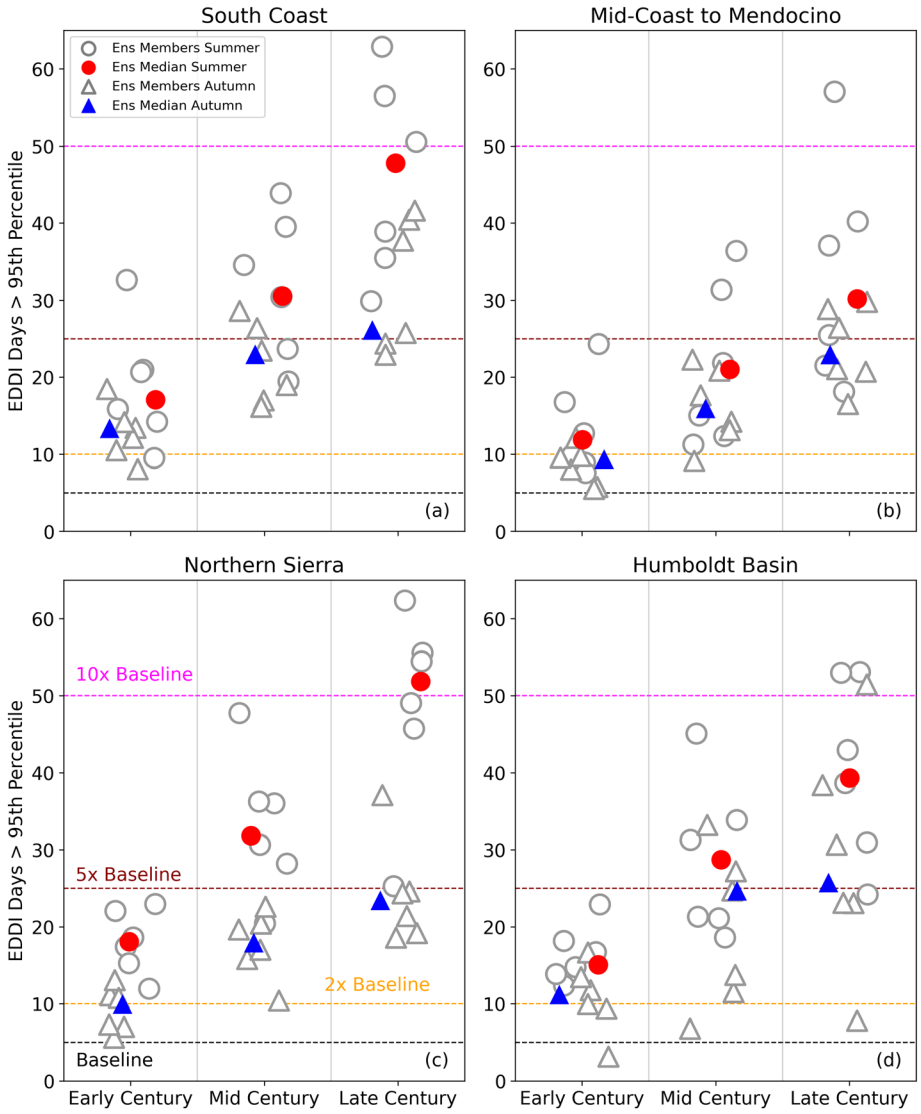

Figure 6. Projected early century (2020–2039), mid century (2040–2069), and late century (2070–2099) RCP 8.5 changes in summer and autumn daily 2-week EDDI exceeding the 95th percentile at (a) South Coast PSA, (b) Mid Coast PSA, (c) Northern Sierra PSA, and (d) Humboldt Basin PSA. Number of seasonal days (n = 91 for autumn) above the 95th percentile is computed for each year and then averaged over each future period. Open circles and triangles indicate LOCA ensemble members for summer and autumn, respectively, and filled circles and triangles are the ensemble medians for summer and autumn, respectively. Black dashed line indicates the baseline or expected number of days per years for the 1950–2019 baseline period, orange dashed line shows 2× the baseline, dark red dashed line shows 5× the baseline, and magenta dashed line shows 10× the baseline.

everywhere except Mid Coast (Figure 7b), highlighting the exacerbated drought severity from recent warming and increased ET_0.

Consecutive drought years are more harmful to ecosystems and water infrastructure than isolated years. At South Coast (Figure 7a) all SPEI-36 values <fifth percentile occurred between 2008 and 2018 with two consecutive years during 2008–2009 and three consecutive years for both SPEI and SPI—the only 3-year period—during 2014–2016. Two consecutive years also occurred 2014–2015 in the Northern Sierra region (Figure 7c). Note that the aggregation window of 36 months makes consecutive years below the fifth percentile more likely.

The fraction of years for each future period with 36-month SPI and SPEI less than the historical fifth percentile value (SPI_5 and $SPEI_5$, respectively) at each PSA is shown in Figure 8 (Figure S9 RCP 4.5). $SPEI_5$ was

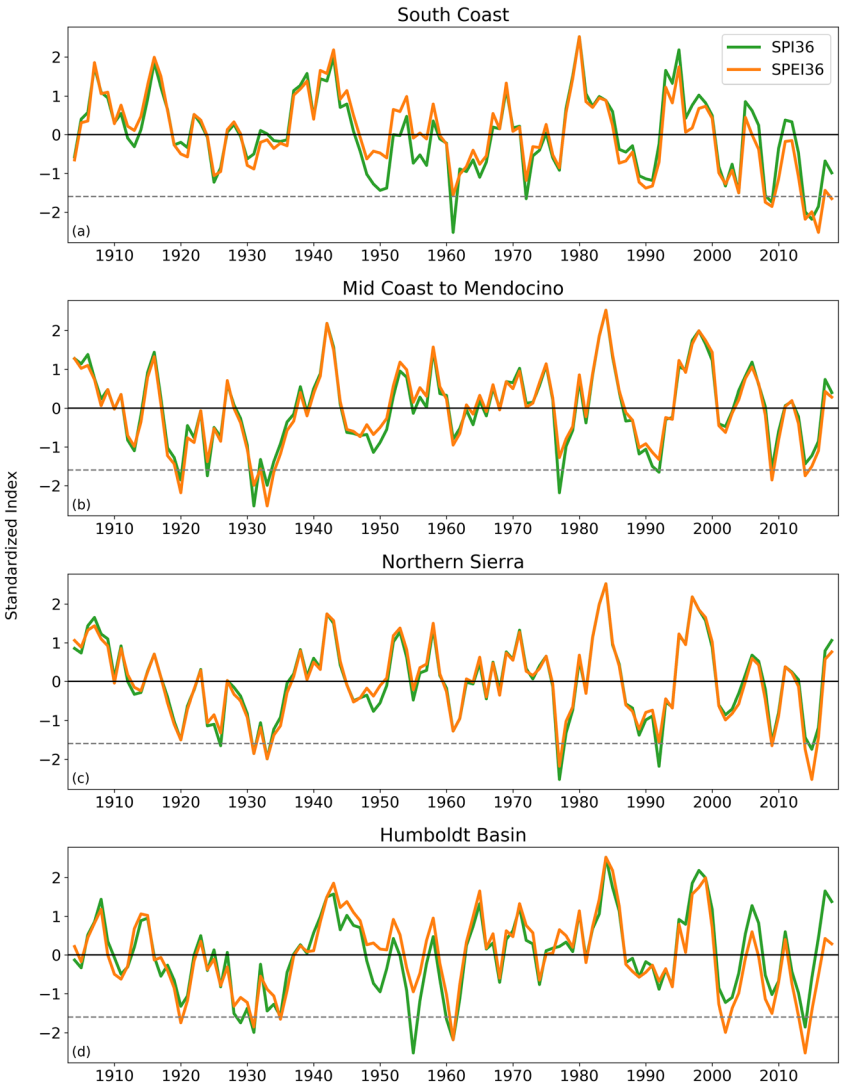

Figure 7. Historical 36-month SPI (green) and SPEI (orange) for the period 1904–2018 at (a) South Coast, (b) Mid Coast, (c) Northern Sierra, and (d) Humboldt Basin. Dashed gray line shows the 5th percentile. Precipitation and ET_0 data from Williams et al. (2020).

found to generally increase through the 21st century with late century ensemble medians ranging from 17% to 73% with South Coast and Humboldt Basin having notably higher $SPEI_5$ compared to Mid Coast and Northern Sierra. Far more limited changes were found in SPI_5. Distinctly large gaps between ensemble median SPI_5 and $SPEI_5$ were found for late century at South Coast and Humboldt Basin. Much smaller differences between $SPEI_5$ and SPI_5 were found at Mid Coast to Mendocino and Northern Sierra even for late century, although $SPEI_5$ almost always exceeded SPI_5, and late century $SPEI_5$ was still notable at 23% and 17% for Mid Coast to Mendocino and Northern Sierra ensemble medians, respectively. The more arid climate of South Coast and Humboldt Basin, where the $Prcp - ET_0$ balance is dominated by ET_0, and the large future changes in ET_0 relative to $Prcp$ at these locations result in far greater changes in $SPEI_5$ compared to SPI_5.

To further examine future changes in multiyear droughts the timeseries of $SPEI_5$ and SPI_5 for the South Coast is shown in Figure 9, and we summarize the late century counts (total numbers of values for a given period), events where an event is defined as two or more years in a row below the fifth percentile, and average duration of those events in Table 2 (early and mid century numbers shown in Tables S1 and S2, respectively). Minimal changes are found in early century $SPEI_5$ counts (Table S1), but by mid century a sharp

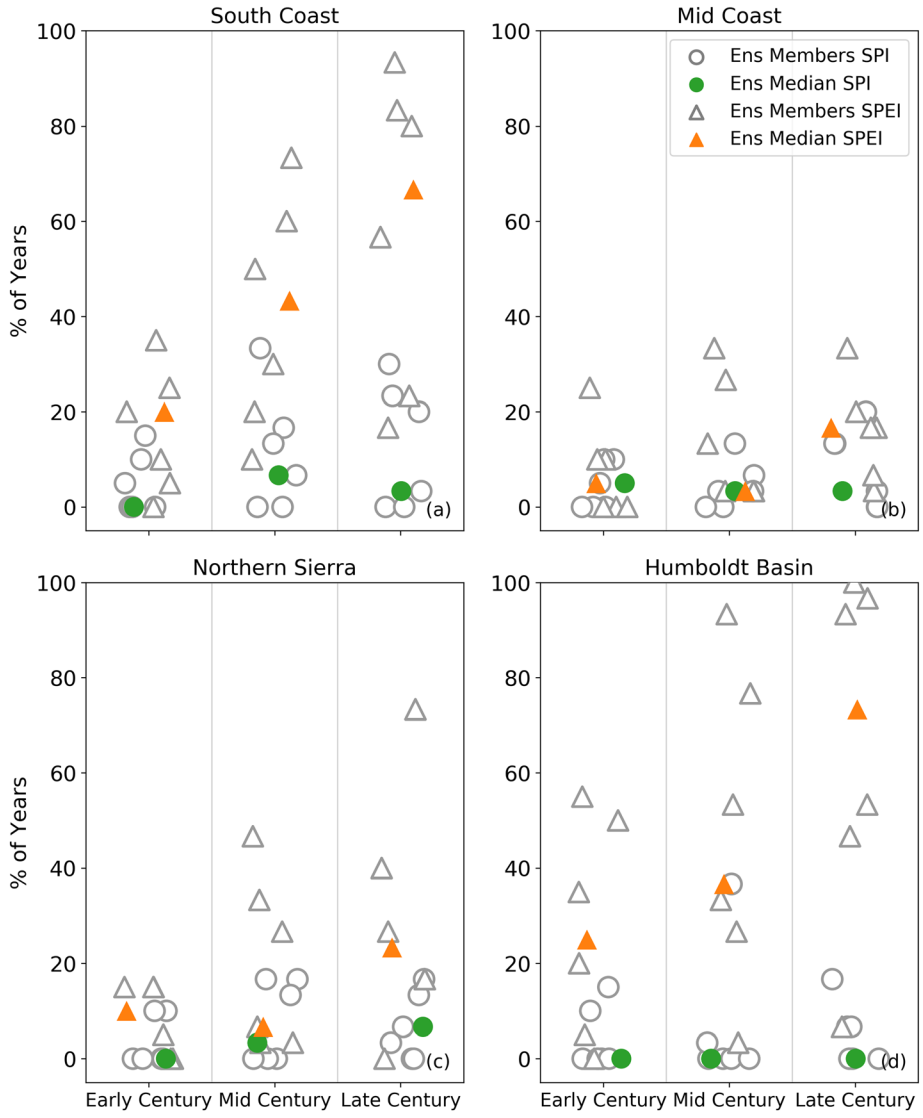

Figure 8. Projected RCP 8.5 changes in extreme multiyear droughts based on a fraction of years when 36-month SPI and 36-month SPEI ending September 30 (end of water year) is below the fifth percentile for (a) South Coast, (b) Mid Coast, (c) Northern Sierra, and (d) Humboldt Basin. Open circles and triangles indicate LOCA ensemble members for SPI and SPEI, respectively, and filled circles and triangles are the ensemble medians for SPI and SPEI, respectively.

increase can be seen in Figure 9a (Table S2) starting around 2040 for most of the LOCA ensemble members. For SPI_5 (Figure 9b) far fewer long duration events were found. However, several ensemble members do indicate increases in both SPI_5 counts and duration of events by late century.

4. Discussion

Consistent with recent studies investigating future changes in California *Prcp* variability and extremes (e.g., Gershunov et al., 2019; Pierce et al., 2013; Swain et al., 2018), we find projected increases in total *Prcp* during winter and decreases during the shoulder seasons of spring and autumn for much of California. For the less studied Nevada, similar patterns of *Prcp* change are found, but those for spring and autumn also show increases for the northern (particularly the northeast) part of the state. For ET_0, our analysis contributes to new insight on the magnitude of change and spatial patterns at seasonal timescales based on high resolution projections.

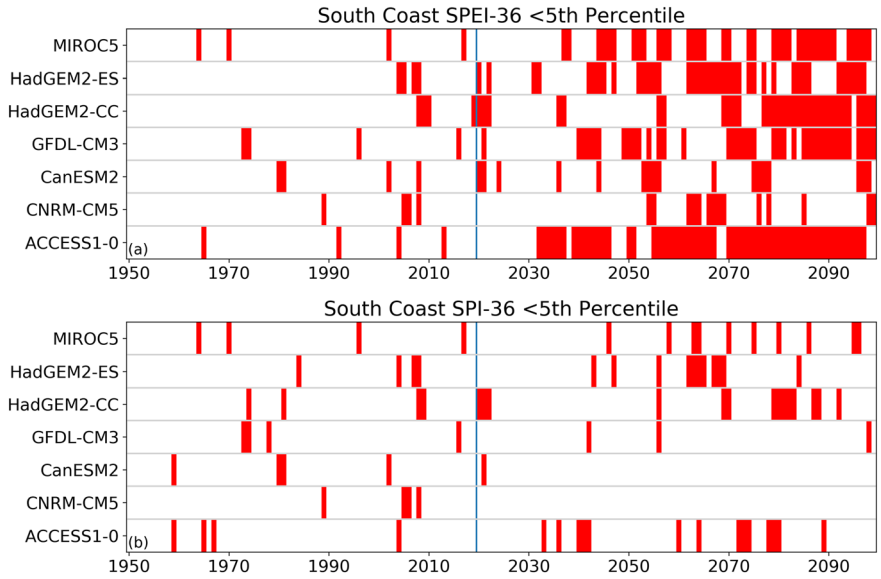

Figure 9. LOCA historical and future RCP 8.5 timeseries of extreme (<fifth percentile relative to 1950–2019 base period) 36-month (a) SPEI and (b) SPI at the South Coast PSA. Individual years below the extreme threshold are represented by single red bars.

Seasonal changes in ET_0 strongly reflect warming T_{mean} with steady increases through the end of the 21st century. This is in contrast to steadily increasing q which give a tendency towards decreasing ET_0. A sensitivity experiment revealed the strong increases in future ET_0 are driven predominantly by increasing T_{mean}. Influences from q were also evident, though not as strong as T_{mean} influences, and the main impact of q was limiting further increasing ET_0, a compensating effect that could not be seen by simply looking at the future ET_0 trends. This further adds to the literature on the importance of using physically based E_0 over simple temperature-based approaches, which in this case would have misrepresented the partially compensating tendencies due to T_{mean} and q. Another consideration is whether the sensitivity of ET_0 to the drivers might change in the future, which could be found by repeating the work of Hobbins (2016) but using future climatology periods instead of past.

Table 2
LOCA South Coast Late Century 36-Month SPEI and SPI Statistics for Values Less Than the Fifth Percentile

SPEI-36 late century <fifth percentile stats				
	Counts (n = 30)	Fraction of years	Events	Average duration (years)
ACCESS1-0	28	0.93	1	28
CNRM-CM5	5	0.17	4	1
CanESM2	7	0.23	2	4
GFDL-CM3	24	0.80	5	5
HadGEM2-CC	25	0.83	3	8
HadGEM2-ES	17	0.57	6	3
MIROC5	20	0.67	5	4
SPI-36 late century <fifth percentile stats				
	Counts (n = 30)	Fraction of years	Events	Average duration (years)
ACCESS1-0	7	0.23	3	2
CNRM-CM5	0	0	0	0
CanESM2	0	0	0	0
GFDL-CM3	1	0.03	1	1
HadGEM2-CC	9	0.30	4	2
HadGEM2-ES	1	0.03	1	1
MIROC5	6	0.20	5	1

Note. An event is defined as two or more years in a row below the fifth percentile.

Considering first 2-week EDDI, recent years with high counts of $EDDI_{95}$ days at Mid Coast and Northern Sierra occurred during the same years with the largest and most destructive wildfires in California's history prior to 2020 (Calfire, 2020a, 2020b), which agrees with the uptick in extreme fire danger found by Goss et al. (2020). In other cases and regions large fires did occur in years with low number of $EDDI_{95}$ days (or zero), which indicates that fires can occur without short-term excess in ET_0 especially when factors other than short-term climate play a key role in the fire potential and spread. In general for California and Nevada, especially in summer and autumn, if extended periods of elevated ET_0 occur simultaneously with *Prcp* deficits the fire danger will increase.

By late century and relative to the historical baseline ensemble median $EDDI_{95}$ days were found to increase 6–10 times in summer and 4–6 times in autumn, which is a much larger increase in extreme days compared to the doubling of autumn days with Fire Weather Index (FWI) values exceeding the 95th percentile by Goss et al. (2020). The FWI is part of the Canadian fire danger system and considers both fire weather and aridity of fuels (Goss et al., 2020). The FWI and EDDI represent different aspects of fire danger with $EDDI_{95}$ day counts representing more of a sustained high fire potential over time compared to the shorter weather timescales incorporated into FWI. In autumn, the average number of days per year with $EDDI_{95}$ by late century is similar to those during destructive 2017 and 2018 autumn fire seasons in northern California regions. However in summer, the median counts far exceed anything found in the observed period used in this study, with the greatest spread between summer and autumn found at South Coast and Northern Sierra. Greater $EDDI_{95}$ counts in summer compared to autumn could be a result of ET_0 being less sensitive to q during summer and more sensitive to T_{mean} which allows for further increased ET_0. This analysis is not sensitive to EDDI timescale as similar results were found using both 1- and 3-month $EDDI_{95}$ days (Figures S10 and S11).

Turning towards the longer timescales, regional differences in 36-month SPI versus SPEI projections in multiyear droughts can be mostly attributed to how water limited regional hydroclimates are (e.g., Vicente-Serrano et al., 2015). At Mid Coast and Northern Sierra there is a close balance between average water year total *Prcp* and ET_0 (less water limited) while at South Coast and Humboldt Basin water year total ET_0 far exceeds *Prcp*. With winter *Prcp* projected to increase (when most of the water year precipitation falls) and ET_0 also projected to increase, the wetting (*Prcp*) and drying (ET_0) tend to continue to balance in less water-limited regions. At more water-limited locations, increased drying is projected (far more extreme droughts in 36-month SPEI than 36-month SPI) as ET_0 already dominates the *Prcp*-ET_0 balance. For South Coast, a shift towards an even more water-limited regime is projected due to substantial decreases in spring and autumn *Prcp* (20–40%) combined with increased ET_0 that will further expand the imbalance between the two. Our results suggest that more multiyear droughts like the recent 2012–2016 drought will be found in the future, when even modest *Prcp* deficits are exacerbated through increased ET_0 and land surface drying (Shukla et al., 2015; Williams et al., 2015).

Increased frequency of extreme multiyear droughts (36-month SPEI) by the end of the century, even at Mid Coast and Northern Sierra, could further increase short-term, seasonal fire danger. Long-term droughts can degrade forests and other ecosystems; however, regional responses can vary substantially. Dong et al. (2019) found major declines in vegetation greenness for southern California in response to the 2012–2016 drought but increases in greenness in northern California and high elevations of the Sierra Nevada. In places where vegetation health decreases, fire danger will increase due to lower fuel moisture and higher flammability. These long-term drought impacts coupled with more extreme 2-week EDDI days and decreasing autumn *Prcp* will further increase fire danger during the autumn.

One uncertainty is the role of increasing carbon dioxide (CO2) on plant physiology and how that could change ET_0. Some argue that increasing CO2 will increase vegetation surface resistance and decrease plant water use, and using a fixed surface resistance for E_0 (such as the ET_0 used in this study) might overestimate future ET_0 and related drought impacts (e.g., Milly & Dunne, 2016, 2017; Roderick et al., 2015; Swann et al., 2016; Yang et al., 2019). Simple adjustments can be applied to surface resistance in the ET_0 equation based on projected CO2 values (Yang et al., 2019). Vicente-Serrano et al. (2020) show that globally, when ET_0 is adjusted for rising CO2, annual values are reduced, but the trend is still increasing for both RCP 4.5 and 8.5. For California and Nevada, the same holds true with increasing ET_0 for both CO2-adjusted (based on Yang et al., 2019) and unadjusted estimates (Figure S12). Although we acknowledge this concern, experiments on actual vegetative responses to elevated CO2 find minimal or no drought reducing effects on

various types of vegetation and ecosystems (e.g., Bachofen et al., 2018; Birami et al., 2020; Dikšaitytė et al., 2019; Duan et al., 2014; Jiang et al., 2020; Nackley et al., 2018). Furthermore, the 2012–2016 extreme hot drought in California and Nevada, intensified by CO2 driven warming (e.g., Shukla et al., 2015; Williams et al., 2015), resulted in major declines in vegetative health for parts of California (Dong et al., 2019) further calling into question whether future CO2 increases will mitigate drying, drought, and fire danger.

Based on a seven-member LOCA downscaled GCM ensemble we show that for California and Nevada, ET_0 will steadily increase through the end of century for all seasons under both RCP 8.5 and 4.5 (Figure S5) scenarios. This will stress native ecosystems, increase fire danger, negatively impact agriculture where water demands cannot be met, and exacerbate impacts to society during periods of prolonged dryness. Projected *Prcp* changes vary with region and season, with notable increases during winter (whole region) and autumn (central and northern Nevada). During these seasons at these locations, a combination of increasing ET_0 and increasing *Prcp* confounds fire danger signals; in that case, the timing of individual *Prcp* events and atmospheric drying events (e.g., heat waves and Santa Ana winds) might play the greatest role in determining fire potential. Conversely, in most of California a clear signal of increased fire potential is expected during autumn with projected increases in ET_0 and decreases in *Prcp*.

The future projections of ET_0 discussed here expand our understanding of possible drought and wildfire potential in California and Nevada, providing resource managers with a more holistic view of possible future scenarios. The regional differences revealed in this analysis demonstrate how future drying may vary across California and Nevada and the need for regionally focused climate change impact and adaptation assessment. Similar analysis could easily be applied to other areas around the globe, where drought and wildfire have significant impacts, to gain more insight into future changes in ET_0 and climatic water balance components at regionally applicable timescales.

Conflict of Interest

The authors declare that they have no conflicts of interest.

Data Availability Statement

All data used in this analysis are publically available through the links as follows: gridMET (http://www.climatologylab.org/gridmet.html); LOCA (http://loca.ucsd.edu); Williams et al. (2020) precipitation and ET_0 (https://www.ldeo.columbia.edu/~williams/megadrought/climate/0.25deg_monthly/multiproduct_1901_2018/observed/).

Acknowledgments
Funding to support this work comes from the National Oceanic and Atmospheric Administration (NOAA) California-Nevada Climate Applications Program under award # NA17OAR4310284 and NOAA National Integrated Drought Information System California-Nevada Drought Early Warning System under award # AB-133E-16-CQ-0022/T0009.

References

Abatzoglou, J. T. (2013). Development of gridded surface meteorological data for ecological applications and modelling. *International Journal of Climatology*, *33*(1), 121–131. https://doi.org/10.1002/joc.3413

Abatzoglou, J. T., & Kolden, C. A. (2013). Relationships between climate and macroscale area burned in the western United States. *International Journal of Wildland Fire*, *22*(7), 1003–1020. https://doi.org/10.1071/WF13019

Abatzoglou, J. T., & Williams, A. P. (2016). Impact of anthropogenic climate change on wildfire across western US forests. *Proceedings of the National Academy of Sciences*, *113*(42), 11,770–11,775. https://doi.org/10.1073/pnas.1607171113

Abatzoglou, J. T., Williams, A. P., & Barbero, R. (2019). Global emergence of anthropogenic climate change in fire weather indices. *Geophysical Research Letters*, *46*, 326–336. https://doi.org/10.1029/2018GL080959

Bachofen, C., Moser, B., Hoch, G., Ghazoul, J., & Wohlgemuth, T. (2018). No carbon "bet hedging" in pine seedlings under prolonged summer drought and elevated CO 2. *Journal of Ecology*, *106*(1), 31–46. https://doi.org/10.1111/1365-2745.12822

Birami, B., Nägele, T., Gattmann, M., Preisler, Y., Gast, A., Arneth, A., & Ruehr, N. K. (2020). Hot drought reduces the effects of elevated CO2 on tree water use efficiency and carbon metabolism. *New Phytologist*. https://doi.org/10.1111/nph.16471

Brown, T., Leach, S., Wachter, B., & Gardunio, B. (2020). The extreme 2018 northern California fire season. *Bulletin of the American Meteorological Society*, *101*(1), S1–S4. https://doi.org/10.1175/BAMS-D-19-0275.1

Brown, T. J., Hall, B. L., & Westerling, A. L. (2004). The impact of twenty-first century climate change on wildland fire danger in the western United States: An applications perspective. *Climatic Change*, *62*(1–3), 365–388.

Calfire (2020a). *Top 20 largest California wildfires*. https://www.fire.ca.gov/media/11416/top20_acres.pdf

Calfire (2020b). *Top 20 most destructive California wildfires*. https://www.fire.ca.gov/media/11417/top20_destruction.pdf

Cayan, D., & Tyree, M. (2015). *Global Climate Model Selection, in Perspectives and Guidance for Climate Change Analysis*, Edited by E. California Department of Water Resources: Lynn and W. O'Daly.

Cayan, D. R., Das, T., Pierce, D. W., Barnett, T. P., Tyree, M., & Gershunov, A. (2010). Future dryness in the southwest US and the hydrology of the early 21st century drought. *Proceedings of the National Academy of Sciences*, *107*(50), 21,271–21,276. https://doi.org/10.1073/pnas.0912391107

Cook, B. I., Smerdon, J. E., Seager, R., & Coats, S. (2014). Global warming and 21st century drying. *Climate Dynamics*, *43*(9–10), 2607–2627. https://doi.org/10.1007/s00382-014-2075-y

Dai, A. (2011). Drought under global warming: A review. *Wiley Interdisciplinary Reviews: Climate Change*, *2*(1), 45–65. https://doi.org/10.1002/wcc.81

Dewes, C. F., Rangwala, I., Barsugli, J. J., Hobbins, M. T., & Kumar, S. (2017). Drought risk assessment under climate change is sensitive to methodological choices for the estimation of evaporative demand. *PLoS ONE*, *12*(3), e0174045. https://doi.org/10.1371/journal.pone.0174045

Dikšaitytė, A., Viršilė, A., Žaltauskaitė, J., Januškaitienė, I., & Juozapaitienė, G. (2019). Growth and photosynthetic responses in Brassica napus differ during stress and recovery periods when exposed to combined heat. *drought and elevated CO2. Plant Physiology and Biochemistry*, *142*, 59–72. https://doi.org/10.1016/j.plaphy.2019.06.026

Dong, C., MacDonald, G. M., Willis, K., Gillespie, T. W., Okin, G. S., & Williams, A. P. (2019). Vegetation responses to 2012–2016 drought in Northern and Southern California. *Geophysical Research Letters*, *46*, 3810–3821. https://doi.org/10.1029/2019GL082137

Duan, H., Duursma, R. A., Huang, G., Smith, R. A., Choat, B., O'GRADY, A. P., & Tissue, D. T. (2014). Elevated [CO 2] does not ameliorate the negative effects of elevated temperature on drought-induced mortality in E ucalyptus radiata seedlings. *Plant, Cell & Environment*, *37*(7), 1598–1613. https://doi.org/10.1111/pce.12260

Farahmand, A., & AghaKouchak, A. (2015). A generalized framework for deriving nonparametric standardized drought indicators. *Advances in Water Resources*, *76*, 140–145.

Ficklin, D. L., Abatzoglou, J. T., Robeson, S. M., & Dufficy, A. (2016). The influence of climate model biases on projections of aridity and drought. *Journal of Climate*, *29*(4), 1269–1285. https://doi.org/10.1175/JCLI-D-15-0439.1

Gershunov, A., Shulgina, T., Clemesha, R. E., Guirguis, K., Pierce, D. W., Dettinger, M. D., et al. (2019). Precipitation regime change in Western North America: The role of atmospheric rivers. *Scientific Reports*, *9*(1), 1–11. https://doi.org/10.1038/s41598-019-46169-w

Goss, M., Swain, D. L., Abatzoglou, J. T., Sarhadi, A., Kolden, C., Williams, A. P., & Diffenbaugh, N. S. (2020). Climate change is increasing the risk of extreme autumn wildfire conditions across California. *Environmental Research Letters*. https://doi.org/10.1088/1748-9326/ab83a7

Griffin, D., & Anchukaitis, K. J. (2014). How unusual is the 2012–2014 California drought? *Geophysical Research Letters*, *41*, 9017–9023. https://doi.org/10.1002/2014GL062433

Hobbins, M., McEvoy, D., & Hain, C. (2017). *Evapotranspiration, Evaporative Demand, and Drought* (pp. 259–287). Drought and Water Crises: Integrating Science, Management, and Policy. https://doi.org/10.1201/b22009-14

Hobbins, M. T. (2016). The variability of ASCE standardized reference evapotranspiration: A rigorous, CONUS-wide decomposition and attribution. *Transactions of the ASABE*, *59*(2), 561–576. https://doi.org/10.13031/trans.59.10975

Hobbins, M. T., Wood, A., McEvoy, D. J., Huntington, J. L., Morton, C., Anderson, M., & Hain, C. (2016). The evaporative demand drought index. Part I: Linking drought evolution to variations in evaporative demand. *Journal of Hydrometeorology*, *17*(6), 1745–1761. https://doi.org/10.1175/JHM-D-15-0121.1

Huntington, J. L., Gangopadhyay, S., Spears, M., Allen, R., King, D., Morton, C., et al. (2015). West-Wide Climate Risk Assessments: Irrigation Demand and Reservoir Evaporation Projections, US Bureau of Reclamation (No. 68-68210, p. 01). Technical memorandum.

Huntington, J. L., Hegewisch, K. C., Daudert, B., Morton, C. G., Abatzoglou, J. T., McEvoy, D. J., & Erickson, T. (2017). Climate engine: Cloud computing and visualization of climate and remote sensing data for advanced natural resource monitoring and process understanding. *Bulletin of the American Meteorological Society*, *98*(11), 2397–2410. https://doi.org/10.1175/BAMS-D-15-00324.1

Jiang, M., Medlyn, B. E., Drake, J. E., Duursma, R. A., Anderson, I. C., Barton, C. V., et al. (2020). The fate of carbon in a mature forest under carbon dioxide enrichment. *Nature*, *580*(7802), 227–231. https://doi.org/10.1038/s41586-020-2128-9

Littell, J. S., Peterson, D. L., Riley, K. L., Liu, Y., & Luce, C. H. (2016). A review of the relationships between drought and forest fire in the United States. *Global Change Biology*, *22*(7), 2353–2369. https://doi.org/10.1111/gcb.13275

Lund, J., Medellin-Azuara, J., Durand, J., & Stone, K. (2018). Lessons from California's 2012–2016 drought. *Journal of Water Resources Planning and Management*, *144*(10) 04018067. https://doi.org/10.1061/(ASCE)WR.1943-5452.0000984

Marshall, A. M., Abatzoglou, J. T., Link, T. E., & Tennant, C. J. (2019). Projected changes in interannual variability of peak snowpack amount and timing in the Western United States. *Geophysical Research Letters*, *46*, 8882–8892. https://doi.org/10.1029/2019GL083770

McEvoy, D. J., Hobbins, M., Brown, T. J., VanderMolen, K., Wall, T., Huntington, J. L., & Svoboda, M. (2019). Establishing relationships between drought indices and wildfire danger outputs: A test case for the California-Nevada drought early warning system. *Climate*, *7*(4), 52. https://doi.org/10.3390/cli7040052

McEvoy, D. J., Huntington, J. L., Abatzoglou, J. T., & Edwards, L. M. (2012). An evaluation of multiscalar drought indices in Nevada and Eastern California. *Earth Interactions*, *16*(18), 1–18. https://doi.org/10.1175/2012EI000447.1

McEvoy, D. J., Huntington, J. L., Hobbins, M. T., Wood, A., Morton, C., Anderson, M., & Hain, C. (2016). The evaporative demand drought index. Part II: CONUS-wide assessment against common drought indicators. *Journal of Hydrometeorology*, *17*(6), 1763–1779. https://doi.org/10.1175/JHM-D-15-0122.1

Milly, P. C., & Dunne, K. A. (2016). Potential evapotranspiration and continental drying. *Nature Climate Change*, *6*(10), 946–949. https://doi.org/10.1038/nclimate3046

Milly, P. C. D., & Dunne, K. A. (2017). A hydrologic drying bias in water-resource impact analyses of anthropogenic climate change. *Journal of the American Water Resources Association*, *53*(4), 822–838. https://doi.org/10.1111/1752-1688.12538

Monteith, J. L. (1965). Evaporation and environment. In Symposia of the society for experimental biology (Vol. 19, pp. 205–234). Cambridge University Press (CUP) Cambridge.

Nackley, L. L., Betzelberger, A., Skowno, A., West, A. G., Ripley, B. S., Bond, W. J., & Midgley, G. F. (2018). CO2 enrichment does not entirely ameliorate Vachellia karroo drought inhibition: A missing mechanism explaining savanna bush encroachment. *Environmental and Experimental Botany*, *155*, 98–106. https://doi.org/10.1016/j.envexpbot.2018.06.018

Nauslar, N., Brown, T. J., McEvoy, D. J., & Lareau, N. (2019). Record setting 2018 California wildfires [in "State of the Climate in 2018"]. *Bulletin of the American Meteorological Society*, *100*(9), S195–S196. https://doi.org/10.1175/2019BAMSStateoftheClimate.1

Nauslar, N. J., Abatzoglou, J. T., & Marsh, P. T. (2018). The 2017 North Bay and Southern California fires: A case study. *Fire*, *1*(1), 18. https://doi.org/10.3390/fire1010018

Oakely, N. S., Hatchett, B. J., McEvoy, D. J., & Rodrigues, L. (2019). *Projected changes in Ventura County Climate*. Reno, NV: Western Regional Climate Center, Desert Research Institute. Retrieved from http://wrcc.dri.edu/Climate/reports.php

Pierce, D. W., & Cayan, D. R. (2016). Downscaling humidity with localized constructed analogs (LOCA) over the conterminous United States. *Climate Dynamics*, *47*(1–2), 411–431. https://doi.org/10.1007/s00382-015-2845-1

Pierce, D. W., Cayan, D. R., Maurer, E. P., Abatzoglou, J. T., & Hegewisch, K. C. (2015). Improved bias correction techniques for hydrological simulations of climate change. *Journal of Hydrometeorology*, *16*(6), 2421–2442. https://doi.org/10.1175/JHM-D-14-0236.1

Pierce, D. W., Cayan, D. R., & Thrasher, B. L. (2014). Statistical downscaling using localized constructed analogs (LOCA). *Journal of Hydrometeorology*, *15*(6), 2558–2585. https://doi.org/10.1175/JHM-D-14-0082.1

Pierce, D. W., Das, T., Cayan, D. R., Maurer, E. P., Miller, N. L., Bao, Y., et al. (2013). Probabilistic estimates of future changes in California temperature and precipitation using statistical and dynamical downscaling. *Climate Dynamics*, *40*(3–4), 839–856. https://doi.org/10.1007/s00382-012-1337-9

Pierce, D. W., Kalansky, J. F., & Cayan, D. R. (2018). Climate, drought, and sea level rise scenarios for California's Fourth Climate Change Assessment. California energy commission (p. 71). Last accessed 5/5/2020 at https://www.energy.ca.gov/sites/default/files/2019-11/Projections_CCCA4-CEC-2018-006_ADA.pdf

Roderick, M. L., Greve, P., & Farquhar, G. D. (2015). On the assessment of aridity with changes in atmospheric CO2. *Water Resources Research*, *51*, 5450–5463. https://doi.org/10.1002/2015WR017031

Scheff, J., & Frierson, D. M. (2014). Scaling potential evapotranspiration with greenhouse warming. *Journal of Climate*, *27*(4), 1539–1558. https://doi.org/10.1175/JCLI-D-13-00233.1

Shukla, S., Safeeq, M., AghaKouchak, A., Guan, K., & Funk, C. (2015). Temperature impacts on the water year 2014 drought in California. *Geophysical Research Letters*, *42*, 4384–4393. https://doi.org/10.1002/2015GL063666

Svoboda, M., LeComte, D., Hayes, M., Heim, R., Gleason, K., Angel, J., et al. (2002). The drought monitor. *Bulletin of the American Meteorological Society*, *83*(8), 1181–1190. https://doi.org/10.1175/1520-0477-83.8.1181

Swain, D. L. (2015). A tale of two California droughts: Lessons amidst record warmth and dryness in a region of complex physical and human geography. *Geophysical Research Letters*, *42*, 9999–9910. https://doi.org/10.1002/2015GL066628

Swain, D. L., Langenbrunner, B., Neelin, J. D., & Hall, A. (2018). Increasing precipitation volatility in twenty-first-century California. *Nature Climate Change*, *8*(5), 427–433. https://doi.org/10.1038/s41558-018-0140-y

Swann, A. L., Hoffman, F. M., Koven, C. D., & Randerson, J. T. (2016). Plant responses to increasing CO2 reduce estimates of climate impacts on drought severity. *Proceedings of the National Academy of Sciences*, *113*(36), 10,019–10,024. https://doi.org/10.1073/pnas.1604581113

Taylor, K. E., Stouffer, R. J., & Meehl, G. A. (2012). An overview of CMIP5 and the experiment design. *Bulletin of the American Meteorological Society*, *93*(4), 485–498. https://doi.org/10.1175/BAMS-D-11-00094.1

Vicente-Serrano, S. M., Beguería, S., & López-Moreno, J. I. (2010). A multiscalar drought index sensitive to global warming: The standardized precipitation evapotranspiration index. *Journal of Climate*, *23*(7), 1696–1718. https://doi.org/10.1175/2009JCLI2909.1

Vicente-Serrano, S. M., McVicar, T. R., Miralles, D. G., Yang, Y., & Tomas-Burguera, M. (2020). *Unraveling the Influence of Atmospheric Evaporative Demand on Drought and its Response to Climate Change* (p. e632). Wiley Interdisciplinary Reviews: Climate Change. https://doi.org/10.1002/wcc.632

Vicente-Serrano, S. M., Van der Schrier, G., Beguería, S., Azorin-Molina, C., & Lopez-Moreno, J. I. (2015). Contribution of precipitation and reference evapotranspiration to drought indices under different climates. *Journal of Hydrology*, *526*, 42–54. https://doi.org/10.1016/j.jhydrol.2014.11.025

Walter, I. A., Allen, R. G., Elliott, R., Jensen, M. E., Itenfisu, D., Mecham, B., et al. (2000). ASCE's standardized reference evapotranspiration equation. In *Watershed management and operations management 2000* (pp. 1–11). Reston, VA: American Society for Civil Engineers. https://doi.org/10.1061/40499(2000)126

Williams, A. P., Abatzoglou, J. T., Gershunov, A., Guzman-Morales, J., Bishop, D. A., Balch, J. K., & Lettenmaier, D. P. (2019). Observed impacts of anthropogenic climate change on wildfire in California. *Earth's Future*, *7*(8), 892–910. https://doi.org/10.1029/2019EF001210

Williams, A. P., Cook, E. R., Smerdon, J. E., Cook, B. I., Abatzoglou, J. T., Bolles, K., et al. (2020). Large contribution from anthropogenic warming to an emerging north American megadrought. *Science*, *368*(6488), 314–318. https://doi.org/10.1126/science.aaz9600

Williams, A. P., Seager, R., Abatzoglou, J. T., Cook, B. I., Smerdon, J. E., & Cook, E. R. (2015). Contribution of anthropogenic warming to California drought during 2012–2014. *Geophysical Research Letters*, *42*, 6819–6828. https://doi.org/10.1002/2015GL064924

Yang, Y., Roderick, M. L., Zhang, S., McVicar, T. R., & Donohue, R. J. (2019). Hydrologic implications of vegetation response to elevated CO 2 in climate projections. *Nature Climate Change*, *9*(1), 44–48. https://doi.org/10.1038/s41558-018-0361-0

Zhao, T., & Dai, A. (2015). The magnitude and causes of global drought changes in the twenty-first century under a low–moderate emissions scenario. *Journal of Climate*, *28*(11), 4490–4512. https://doi.org/10.1175/JCLI-D-14-00363.1